5th International Symposium on Three-Dimensional Electromagnetics
Sapporo, Japan, May 7-9, 2013

Anisotropic 3D inversion of marine CSEM data

Yutaka Sasaki[1]
[1]Kyushu University

SUMMARY

We present an anisotropic 3D inversion algorithm for marine controlled-source electromagnetic (CSEM) data with the assumption that electrical anisotropy is represented by the vertical and horizontal resistivities. For such anisotropic media, the horizontal and vertical electric fields are related to the horizontal and vertical resistivities, respectively. In addition, as is well-known for magnetotelluric data, the horizontal electric field is insensitive to thin, horizontal resistors associated with the presence of hydrocarbon reservoirs. Thus, the horizontal electric field contributes mainly to defining the horizontal resistivity of the background media, but not resolving thin resistors in the vertical resistivity. As a result, the resolution of marine CSEM data to thin resistors is lower in anisotropic media than that for the isotropic case, unless the possible relationship between the two resistivities is accounted for. We demonstrate using a synthetic example that one can improve the resolution to deep thin resistors significantly in both the vertical and horizontal resistivities by incorporating the equality of the two resistivities into the inversion process. We also show that using multiple-frequency data is important in improving the target and overall resolution.

Keywords: 3D inversion, anisotropy, TIV, marine CSEM

INTRODUCTION

The marine controlled-source electromagnetic (CSEM) surveying has been increasingly used for hydrocarbon exploration in more complex geologic settings. Issues that complicate the interpretation of marine CSEM data include shallow-water problem, formation anisotropy, bathymetric variations, and near-seafloor variations of resistivity. These issues can basically be addressed by implementing a rigorous 3D inversion in which the response from the actual marine environment can be accurately modeled. As for anisotropy, it has been recognized in industry that electrical anisotropy occurs more commonly than considered before and thus inverting CSEM data without taking into account anisotropy can lead to misleading interpretation (e.g., Newman et al., 2010). Hence, there has been a growing effort to implement anisotropic 3D inversion algorithms (Newman et al., 2010; Lovatini et al., 2009; Morten et al., 2010; Wiik et al., 2011; Sasaki, 2011). However, there seems to be no consensus about the capability of anisotropic 3D inversion to detect and delineate reservoirs from CSEM data influenced by anisotropy. This is partly because very few synthetic data studies for deep targets have been presented in the published literature.

The purpose of this study is to demonstrate through 3D inversion of synthetic data how deep, thin resistors representative of reservoirs (more than 2 km below seafloor) can be resolved for different frequencies in various situations. The inversion method is a Gauss-Newton approach and the forward modeling is based on a finite-difference (FD) method that assumes a simple form of anisotropy, referred to as transverse isotropy in the vertical direction (TIV).

INVERSION METHOD

We divide the inversion region into a set of rectangular blocks, and assume that the resistivity is constant in each block. The inverse problem is formulated as a nonlinear least-squares problem where the objective functional to be minimized is

$$\begin{aligned}\phi = &\left\|\mathbf{W}\left[\mathbf{d}-\mathbf{f}(\mathbf{m}_h,\mathbf{m}_v)\right]\right\|^2+\alpha^2\left\|\mathbf{C}\mathbf{m}_h\right\|^2 \\ &+\alpha^2\left\|\mathbf{C}\mathbf{m}_v\right\|+\beta^2\left\|\mathbf{m}_h-\mathbf{m}_v\right\|^2\end{aligned}. \qquad (1)$$

In the above, $\mathbf{m}_h$ and $\mathbf{m}_v$ are, respectively, the logarithms of the horizontal and vertical resistivities, $\mathbf{d}$ is a vector of CSEM data, $\mathbf{f}$ is a forward modeling function, $\mathbf{C}$ is a second-order FD matrix to define the roughness of the horizontal and vertical resistivity distributions, and $\mathbf{W}$ is a diagonal matrix whose elements are the reciprocals of the estimated uncertainty for each datum. The last term in ϕ is added to impose the equality of the horizontal and vertical resistivities. Although seemingly inconsistent with anisotropic inversion, the equality constraint is important in improving the target resolution, as shown later. By using this constraint, anisotropic resistivity is expected to be recovered only when the data demand it. The parameters α and β control the smoothness of the two resistivities and the equality constraint, respectively. The data used in the inversion are the real and imaginary parts of the electric fields for given frequencies and source-receiver

geometries, and are normalized by the electric-field amplitudes.

The inverse problem is iteratively solved by linearizing the function **f** with respect to the starting model parameters and searching for perturbations $\Delta\mathbf{m}_h$ and $\Delta\mathbf{m}_v$. At the *n*-th iteration, the linearized objective functional is

$$\begin{aligned}\phi &= \left\|\mathbf{W}\left[\Delta\mathbf{d} - \mathbf{A}_h\Delta\mathbf{m}_h - \mathbf{A}_v\Delta\mathbf{m}_v\right]\right\|^2 \\ &+ \alpha^2\left\|\mathbf{C}(\mathbf{m}_h^{(n)} + \Delta\mathbf{m}_h)\right\|^2 + \alpha^2\left\|\mathbf{C}(\mathbf{m}_v^{(n)} + \Delta\mathbf{m}_v)\right\|^2, \quad (2) \\ &+ \beta^2\left\|\mathbf{m}_h^{(n)} + \Delta\mathbf{m}_h - \mathbf{m}_v^{(n)} - \Delta\mathbf{m}_v\right\|^2\end{aligned}$$

where $\Delta\mathbf{d}$ is the difference between the observed and predicted data, and $\mathbf{A}_h$ and $\mathbf{A}_v$ are the Jacobians with respect to the horizontal and vertical resistivities, respectively. The minimization of the objective functional is equivalent to obtaining the least-squares solution of the rectangular (or overdetermined) linear system of equations

$$\begin{bmatrix} \mathbf{W}\mathbf{A}_h & \mathbf{W}\mathbf{A}_v \\ \alpha\mathbf{C} & \mathbf{0} \\ \mathbf{0} & \alpha\mathbf{C} \\ \beta\mathbf{I} & -\beta\mathbf{I} \end{bmatrix} \begin{Bmatrix} \Delta\mathbf{m}_h \\ \Delta\mathbf{m}_v \end{Bmatrix} = \begin{Bmatrix} \mathbf{W}\Delta\mathbf{d} \\ -\alpha\mathbf{C}\mathbf{m}_h^{(n)} \\ -\alpha\mathbf{C}\mathbf{m}_v^{(n)} \\ -\beta\mathbf{I}(\mathbf{m}_h^{(n)} - \mathbf{m}_v^{(n)}) \end{Bmatrix}. \quad (3)$$

The least-square solution can be obtained by using the modified Gram-Schmidt method.

SENSITIVITY

The Gauss-Newton approach requires generating the Jacobian to solve the nonlinear least-squares problem, as shown above. Denoting the conductivity within a region *V*, by σ, the sensitivity or the partial derivative of the *x* component of the electric field is given by

$$\frac{\partial E_x}{\partial \sigma} = \int_V \mathbf{E}\cdot\mathbf{E}^J\, dv, \quad (4)$$

where **E** is the electric field within the region of interest due to the actual source, and $\mathbf{E}^J$ is the electric field due to the (fictitious) *x*-directed unit electric dipole placed at the receiving point (e.g., McGillivray et al., 1994). For the case of TIV media, the horizontal component of the electric field depends on the horizontal conductivity, σ_h, whereas the vertical component depends on the vertical conductivity, σ_v. Thus, the partial derivatives become

$$\frac{\partial E_x}{\partial \sigma_h} = \int_V \left(E_x E_x^J + E_y E_y^J\right) dv \quad (5)$$

$$\frac{\partial E_x}{\partial \sigma_v} = \int_V E_z E_z^J\, dv. \quad (6)$$

It is seen from equations (5) and (6) that the sensitivities to the horizontal and vertical conductivities are determined solely by the horizontal and vertical electric fields, respectively. This implies that the sensitivities to the horizontal and vertical conductivities are decoupled, which naturally results in poorer resolution than that for the isotropic case.

SYNTHETIC EXAMPLE

Model

The model used in this study is shown in Figure 1. A reservoir model with dimensions of 5 km x 6 km x 100 m in the *x*, *y*, and *z* directions is embedded in the second layer of a three-layered background structure. The top of the reservoir is located 2 km below the seafloor. The reservoir and the first and second background layers are anisotropic. The reservoir has vertical and horizontal resistivities of 50 and 20 ohm-m. The vertical resistivities of the background layers are 1.5, 2, and 10 ohm-m, while the horizontal resistivities are 1, 1.5, and 10 ohm-m (from the top to the bottom). The third layer (10 ohm-m) represents the isotropic basement and has an escarpment 400 m high. Two near-seafloor slabs with isotropic resistivity of 4 ohm-m simulate hydrate accumulations. The water resistivity is 0.3 ohm-m and its depth is 100 m.

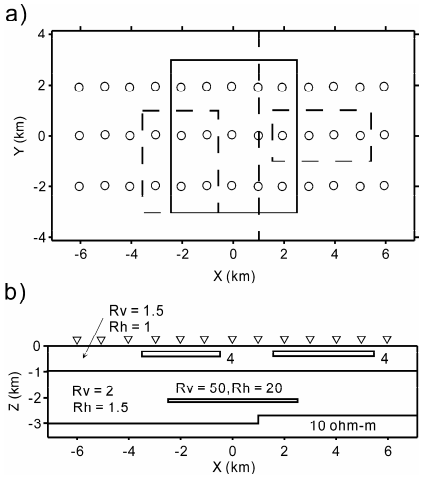

Figure 1. (a) Plan view and (b) vertical cross section along the central line (*y* = 0) of 3D anisotropic subseafloor model used to generate marine CSEM data. The projections of the reservoir and near-seafloor anomalies are indicated by the solid and dashed lines, respectively, in the plan view.

Thirty-nine seafloor receivers that are spaced at 1 km in the *x* direction and 2 km in the *y* direction measure the *x*-directed electric field. A 200-m horizontal electric dipole is assumed to be towed 50 m above the receivers in the *x* direction. There are a total of 48 source locations. Three frequencies are considered: 0.1, 0.3, and 0.5 Hz. The data are acquired for both inline and broadside (offline) geometries, and the total number of data per frequency is 3744. Gaussian noise with a standard deviation of 6% of the electric-field amplitude was added to the model response. In the inversion, the model region was divided

into 5832 (27 x 9 x 24) blocks, and the forward modeling used a FD grid of 87 x 71 x 49 cells. The regularization parameter α was set to values of 1.0, 0.5, and 0.3 for the first three iterations, and 0.2 for the remaining iterations. The parameter β was set to 0.2. The starting model is a 2-ohm-m isotropic half-space (underlying the water layer).

Results

To illustrate the effect of the equality constraint on the inverted images, inversions were first performed excluding the last term in equation (1). Figures 2 and 3 show the vertical and horizontal resistivities, respectively, obtained from single frequencies (0.1, 0.3, and 0.5 Hz) and all frequencies together. In these figures, only the vertical cross section along the central line (y = 0) of the recovered model is shown for each inversion. In all cases, the RMS data misfit converged to a value between 0.057 and 0.059 after four to five iterations. In Figure 2, signatures from the thin resistor can be seen clearly in the vertical resistivity, but its depth resolution is rather poor. Such a result arises from the fact that the sensitivities to the vertical and horizontal resistivities are decoupled for anisotropic media; in other words, the horizontal electric field is directly related to the horizontal resistivity and thus contributes mainly to defining the horizontal resistivity, but not to resolving thin resistors in the vertical resistivity. In the horizontal resistivity (Figure 3), an indication from the target resistor is only slightly visible in multiple-frequency inversion. This is due to the fact that, as is well-known for magnetotelluric data, the horizontal electric field is insensitive to horizontal thin resistors.

The results of anisotropic inversion incorporating the equality constraint are shown in Figures 4 and 5. In all cases, the RMS data misfit converged to a value between 0.057 and 0.062 after four to five iterations. It is evident that the depth resolution is improved for all frequencies in both the vertical and horizontal resistivities. This is because the horizontal components of the electric field contribute to resolving not only the horizontal resistivity of the background media but also the vertical resistivity of the reservoir through the equality constraint.

It is encouraging to see that using multiple frequencies improve the target and overall resolution significantly and that a 2 km-deep reservoir can be clearly detected and imaged for a 100-m water and 6% data noise. However, the high-resistivity zone recovered from multi-frequency inversion is still ~400 m shallower than the actual reservoir depth. Note that a horizontal low-resistivity zone spreads over the high-resistivity zone, which is considered to occur to compensate for the high-resistivity zone being too shallow. This feature is considered to reflect the non-uniqueness of a given inverse problem, but it is possible that it is partly due to the particular inversion algorithm used, especially smoothness constraint that is based on the second-order FD operator.

CONCLUSIONS

A TIV 3D inversion algorithm for marine CSEM data has been developed based on a Gauss-Newton approach and finite-difference modelling. One important feature of anisotropic inversion is that the sensitivities for the horizontal and vertical resistivities are virtually decoupled. Besides, marine CSEM data are insensitive to the horizontal resistivity of thin resistive layers because the horizontal resistivity is related to the horizontal electric field which does not intersect the layer boundaries, causing no appreciable galvanic effects. As a result, the resolution achieved by anisotropic inversion is inherently lower than that for the isotropic case, unless the some relation between the two resistivities is incorporated into inversion. It is shown through a synthetic example that deep, thin resistors can be much better resolved in both the vertical and horizontal resistivities by imposing the equality of the two resistivities. It is also shown that using multiple frequencies is essential in improving the target and overall resolution.

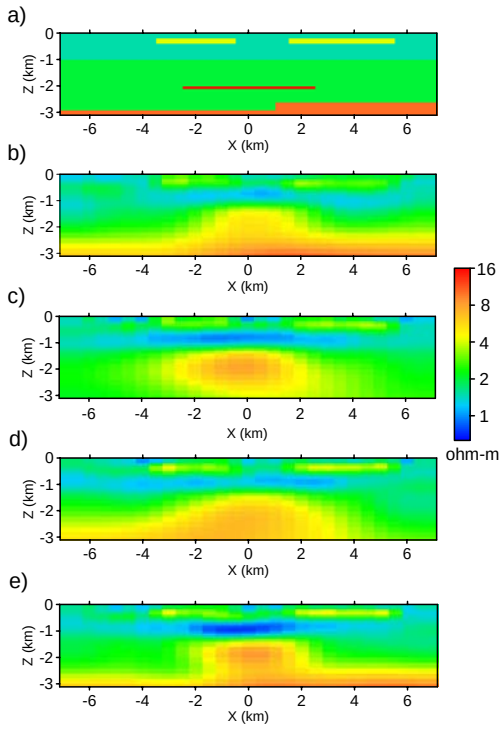

Figure 2. The vertical resistivity cross-section along the central line of the true model (a) and those recovered from 3D inversion for single frequencies of (b) 0.1, (c) 0.3, and (d) 0.5 Hz, and (e) all three frequencies. The equality constraint is not used.

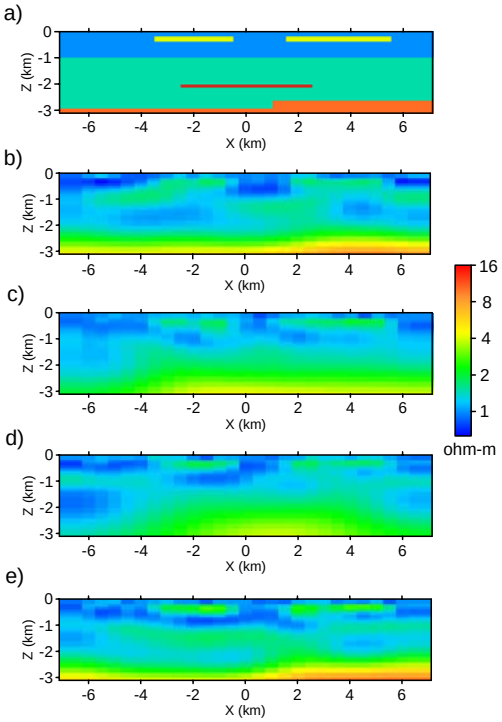

Figure 3. The horizontal resistivity cross-section along the central line of the true model (a) and those recovered from 3D inversion for single frequencies of (b) 0.1, (c) 0.3, and (d) 0.5 Hz, and (e) all three frequencies. The equality constraint is not used.

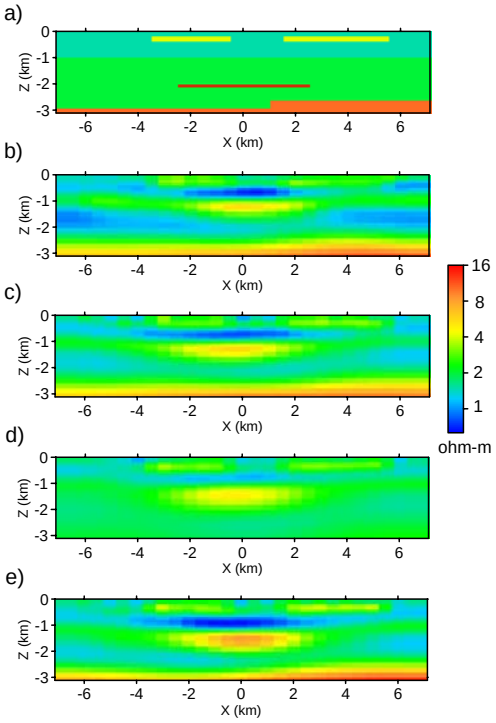

Figure 4. The vertical resistivity cross-section along the central line of the true model (a) and those recovered from 3D inversion for single frequencies of (b) 0.1, (c) 0.3, and (d) 0.5 Hz, and (e) all three frequencies. The equality constraint is used.

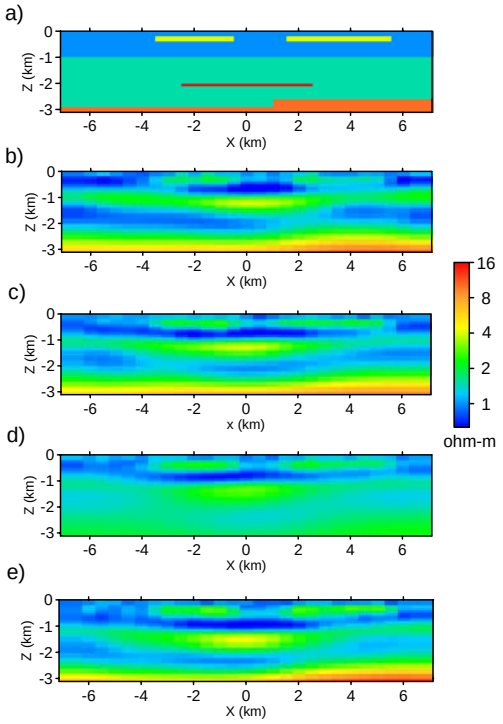

Figure 5. The horizontal resistivity cross-section along the central line of the true model (a) and those recovered from 3D inversion for single frequencies of (b) 0.1, (c) 0.3, and (d) 0.5 Hz, and (e) all three frequencies. The equality constraint is used.

REFERENCES

Lovantini, A., Watts, M. D., Umbach, K. E., Ferster, A., Patmore, S., and Stilling, J., 2009, Application of 3D anisotropic CSEM inversion offshore west of Greenland, *79th Annual International Meeting, SEG, Expanded Abstracts*, 830-834.

McGillivray, P. R., Oldenburg, D. W., Ellis, R. G., and Habashy, T. M., 1994, Calculation of sensitivities for the frequency-domain electromagnetic problem, *Geophysical Journal International*, **116**, 1-4.

Morten, J. P., Bjorke, A. K., and Nguyen, A. K., 2010, Hydrocarbon reservoir thickness resolution in 3D CSEM anisotropic inversion, *80th Annual International Meeting, SEG, Expanded Abstracts*, 599-603.

Newman, G. A., Commer, M., and Carazzone, J. J., 2010, Imaging CSEM data in the presence of electrical anisotropy, *Geophysics*, 7**5**, F51–F61.

Sasaki, Y., 2011, Anisotropic, joint 3D inversion of marine CSEM and MT data, *81st Annual International Meeting, SEG, Expanded Abstracts*, 589-593.

Wiik, T., and Loseth, L. O., Ursin, B., and Hokstad, K., 2011, TIV contrast source inversion of mCSEM data, *Geophysics*, **76**, F65-F7.